

Studies on structural characterization and electrical properties of Cu-doped BiFeO₃ thin films

T Jampreecha^{1,2,3}, J Khajonrit^{3,4}, P Kidkhunthod^{3,4}, W Meevasana^{1,3} and S Maensiri^{1,3}

¹ School of Physics Institute of Science Suranaree University of Technology, Nakhon Ratchasima, 30000, Thailand

² Development and Promotion of Science and Technology Talents Project Royal Government of Thailand Scholarship, Bangkok, 10110, Thailand

³ SUT CoE on Advanced Functional Materials (SUT-AFM), Suranaree University of Technology, Nakhon Ratchasima, 30000, Thailand

⁴ Synchrotron Light Research Institute (Public Organizer), Nakhon Ratchasima, 30000, Thailand

E-mail: tachgiss_off@hotmail.com

Abstract. Cu-doped BiFeO₃ (x = 0, 0.2, 0.3 and 0.5) thin films were fabricated on Pt/Si n-type substrates by a spin coating method. The phase and structure of thin films were characterized by x-ray diffraction (XRD). The homogeneous surface and the film thickness (200-300 nm) of the thin films were investigated by scanning with an electron microscope (SEM). X-ray absorption spectroscopy (XAS) confirmed the presence of the Fe³⁺ and the mixing of Cu²⁺ and Cu³⁺ oxidation states in the thin film samples. The electrical properties were studied with an Agilent4294A impedance analyzer. The influence of Cu-doping with x = 0 to x = 0.3 on the thin films can affect the structure of the thin film with decreasing crystallite sizes (2.9 nm to 2.6 nm), which lead to decreasing grain boundary conductivity (σ_{gb}) (1.1×10^{-4} S/cm to 0.2×10^{-4} S/cm) and increasing grain boundary resistance (R_{gb}) (9.1 k Ω to 35.7 k Ω), respectively. Interestingly, the Cu-doping at x = 0.5 with large crystallite sizes (3.4 nm) can exhibit both low R_{gb} (6.5 k Ω) and high σ_{gb} (1.5×10^{-4} S/cm).

1. Introduction

In recent years perovskite bismuth ferrite (BiFeO₃) has become of interest as a multiferroic material, which exhibits magnetic, electrical and elastic properties and usually exists in an R3c space group [1]. BiFeO₃ has been used in wide applications such as solar cell separators, capacitors, transformers and piezoelectric devices, etc. [2-5]. The magnetic properties of bismuth ferrite nanoparticles were found to be below room temperature [6-7] with saturation magnetization (M_s) of about 0.05 emu/g [8]. Generally, the dielectric constant of BiFeO₃ nanoparticles are found to be about 370 - 170 at a frequency of 0.1-10.0 kHz at room temperature [9-10]. The BiFeO₃ thin films exhibited the M_s value and saturation polarization (P_r) value of about 103 emu/cm³ and 22.0 μ C/cm², respectively [6, 11-12]. Recently, researchers have tried to improve or study its structure and properties using various methods such as doping with ions at Bi or Fe sites [4-5] by synthesis using different methods to obtain various forms, such as nanoparticles, nanorods, nanofibers and thin films [8]. The fabrication of thin films by using a

thin film technique has attracted increasing interest in the modification of their magnetic and electrical properties. Spin coating is an easy technique for thin film preparation which uses sol-gel precursor solution and a spin coating machine. Moreover, doping with Cu, Ni and Co ions in the BiFeO₃-based nanoparticles causes changes to the structure that can improve their magnetic properties [13-14]. Therefore, this research used a spin coating technique to fabricate the Cu-doped BiFeO₃ thin films and chose Cu ion as a substituent to study the effects of Cu addition and to improve their electrical properties. Moreover, the structure characterizations of the prepared thin film samples were investigated by various techniques such as X-ray diffraction (XRD), scanning electron microscope (SEM) and X-ray absorption spectroscopy (XAS). Furthermore, this research investigated the electrical properties to clarify the mechanism underlying the effect of the Cu-doping on the structure and electrical properties of BiFeO₃ thin films.

2. Experimental procedure

2.1. Synthesis of BiFe_{1-x}Cu_xO₃ as x=0.0, 0.2, 0.3 and 0.5 thin films

BiFe_{1-x}Cu_xO₃ (x = 0.0, 0.2, 0.3 and 0.5) thin films were prepared by a simple spin coating method. The precursor solution was prepared by mixing bismuth (III) acetate [Bi(CH₃CO₂)₃, 99.99%, Sigma-Aldrich], iron(II) acetate [Fe(C₂H₃O₂)₂, 99.99%, Sigma-Aldrich] and copper (II) acetate [Cu(CO₂CH₃)₂, 99.99%, Sigma-Aldrich], acetone in acetic acid, acetylacetonone, deionized water and ethylene glycol [7-8, 10, 15]. Initially, 20 ml each of deionized water and ethylene glycol, 10 ml each of acetone and acetylacetonone, and 5 ml of acetic acid were dissolved under a magnetic stirrer at 353 K for 30 min. Then, bismuth (III) acetate, iron (II) acetate and copper (II) acetate were added and stirred at 353 K for 3 h and 392 K for 3 h. Next, the mixture solution was dropped on Pt/Si N-type and spun at 4000 rpm. After that, the BiFe_{1-x}Cu_xO₃ thin films were dried at 423 K for 5 min. Finally, the thin films were annealed at 873 K for 6 h.

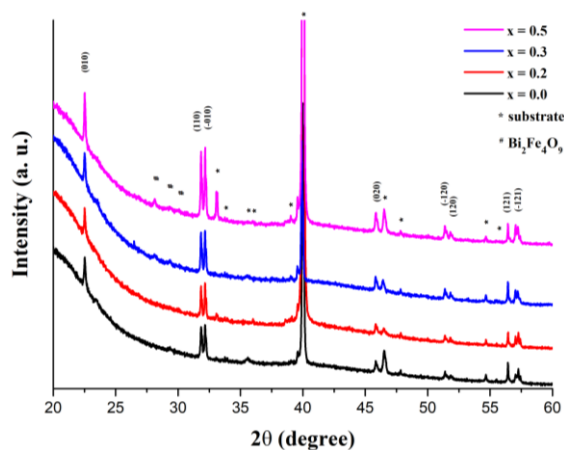


Figure 1. XRD patterns of BiFe_{1-x}Cu_xO₃ thin films (x = 0.0, 0.2, 0.3 and 0.5).

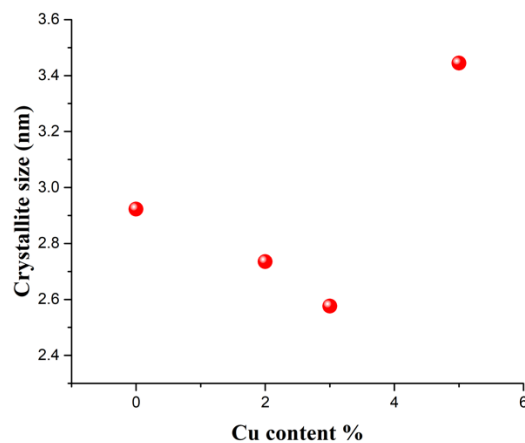


Figure 2. Crystallite sizes versus Cu content of BiFe_{1-x}Cu_xO₃ thin films (x = 0.0, 0.2, 0.3 and 0.5).

2.2. Characterization

The XRD patterns of BiFe_{1-x}Cu_xO₃ thin films were investigated by using X-ray diffraction (XRD; Bruker D8 Advance) analysis with Cu K α at $\lambda \approx 0.15406$ nm. The crystallite size of the prepared thin films was calculated using the Debye-Scherrer equation [8]

$$D = \frac{0.9\lambda}{\beta \cos\theta} \quad (1)$$

where D is crystallite size (nm), β is the full width at half maximum (FWHM) intensity and θ is the diffraction angle. The surface and thickness of the thin films were observed by scanning electron microscopy (SEM; JEOL JSM-7800F). X-ray absorption spectroscopy (XAS) was used to investigate the oxidation state of the thin films. X-ray absorption near-edge structure (XANES) of Cu and Fe K-edge spectra were acquired at the SUT-NANOTEC-SLRI XAS beamline (BL 5.2) at the Synchrotron Light Research Institute (SLRI), Thailand. The XANES data were analyzed using ATHENA software which included an IFEFFIT package [16].

2.3. Measurement of Electrical properties

The electrical properties were measured with an Agilent4294A impedance analyzer over frequency 102-107 Hz on the oscillation voltage of 0.5 volt. The complex impedance spectroscopy Z was calculated by the following equation [17].

$$\varepsilon^* = \varepsilon' - i\varepsilon'' = \frac{1}{i\omega C_0 Z^*} = \frac{1}{i\omega C_0 (Z' - iZ'')} \quad (2)$$

where ω is angular frequency of applied AC electricity, ε' and ε'' are real and imaginary part of dielectric permittivity constant ε^* , Z' and Z'' are real and imaginary part of complex impedance Z^* , respectively. The impedance spectroscopy can be used to describe electrical transport inside grains and grain boundaries of materials by using a brick-work model, where R_g , C_g , σ_g are resistance, capacitance and conductivity of grains and R_{gb} , C_{gb} , σ_{gb} are resistance, capacitance and conductivity of grain boundaries, respectively. The conductivity is related to resistance ($\sigma_{g,gb}$), which is $(\frac{1}{R_{g,gb}})$. The parameters were calculated using the following equation [17].

$$Z^* = Z' - iZ'' = \left(\frac{R_g}{1 + R_g \omega C_g^2} + \frac{R_{gb}}{1 + R_{gb} \omega C_{gb}^2} \right) - i \left(\frac{R_g^2 \omega C_g}{1 + R_g \omega C_g^2} + \frac{R_{gb}^2 \omega C_{gb}}{1 + R_{gb} \omega C_{gb}^2} \right) \quad (3)$$

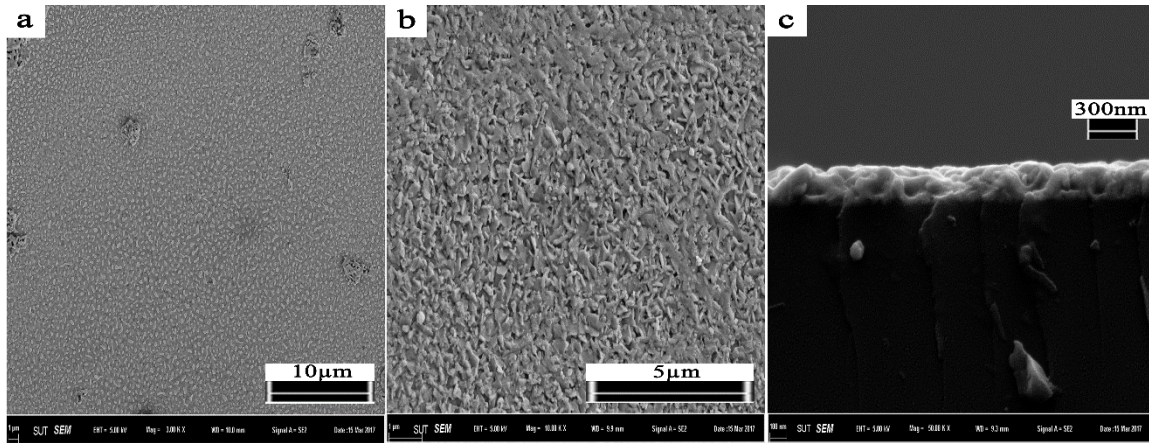


Figure 3. (a, b) SEM and (c) SEM cross-section images of $\text{BiFe}_{1-x}\text{Cu}_x\text{O}_3$ thin films at $x = 0.3$.

3. Results and discussion

3.1. Structure analysis

The XRD patterns of the purity phase of BiFeO_3 (ICSD 15299) for the undoped BiFeO_3 thin films and impurity phases of $\text{Bi}_2\text{Fe}_4\text{O}_9$ (ICSD 15299 and ICSD 20067) for Cu-doped BiFeO_3 thin films [1, 8] are shown in figure 1. The impurity phases occur when Cu is substituted in the BiFeO_3 structure, which can be attributed to the incomplete replacement of Cu at the Fe site. The intensity of the impurity phase increases with increasing Cu concentration. The crystallite sizes of $\text{BiFe}_{1-x}\text{Cu}_x\text{O}_3$ thin films of 2.92, 2.73, 2.57 and 3.44 nm as $x = 0.0, 0.2, 0.3$ and 0.5 are shown in figure 2. The crystallite sizes decrease with increasing Cu contents $x = 0.0, 0.2$ and 0.3 , respectively [8]. Clearly, the decrease in the crystallite

size causes an increase of the Cu content. Except for $x = 0.5$ sample, the increase in the crystallite size may be due to the incomplete replacement of Cu in BiFeO_3 , which causes an increase in the impurity phase of $\text{Bi}_2\text{Fe}_4\text{O}_9$. In this work, the decrease in the crystallite size conforms to the substitution of the Fe^{3+} (7.8 nm) site with smaller ionic radius of Cu^{2+} (5.4 nm) [8]. Figure 3 shows the SEM image revealing the surface and thickness of the thin films. The average film thickness of the thin films is about 200-300 nm. The normalized XANES spectra of all samples at the Fe and Cu K-edge of all samples are shown in figures 4 and 5. The Fe and Cu K-edge XANES spectra of the $\text{BiFe}_{1-x}\text{Cu}_x\text{O}_3$ thin films are compared with standard materials with different Fe and Cu oxidation states. The absorption edge of all samples at the Fe K-edge match with the standard materials of Fe^{3+} and the Cu K-edge is located between the standard materials of Cu^{2+} and Cu^{3+} . Clearly, the oxidation states of Fe and Cu in the Cu-doped BiFeO_3 thin films are 3+ and mixing of 2+ and 3+, respectively [8].

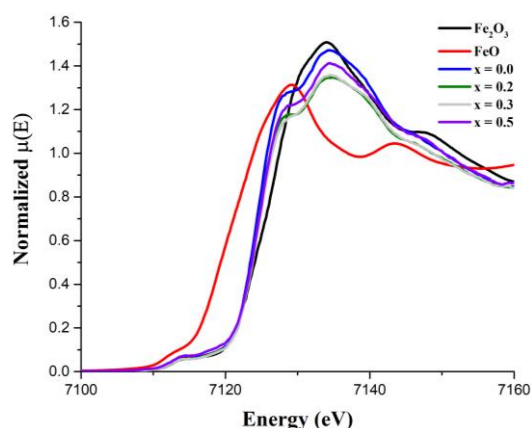


Figure 4. XAS spectra of Fe K-edge of $\text{BiFe}_{1-x}\text{Cu}_x\text{O}_3$ thin films ($x = 0.0, 0.2, 0.3$ and 0.5).

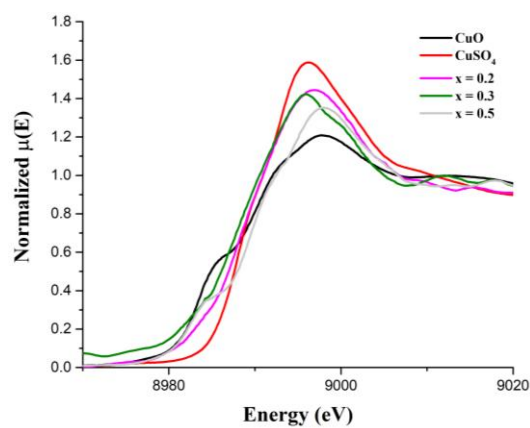


Figure 5. XAS spectra of Cu K-edge of $\text{BiFe}_{1-x}\text{Cu}_x\text{O}_3$ thin films ($x = 0.0, 0.2, 0.3$ and 0.5).

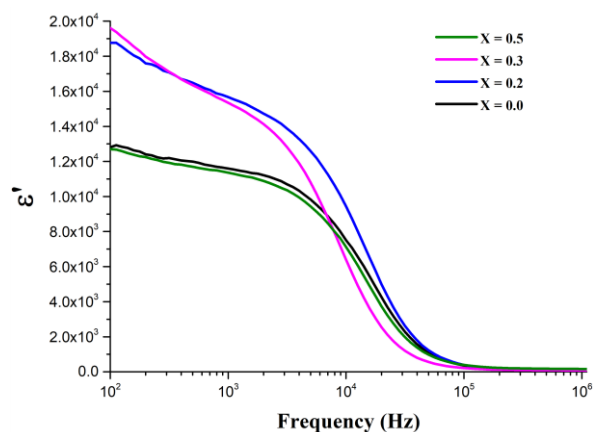


Figure 6. Frequency dependence of real dielectric permittivity (ϵ') of $\text{BiFe}_{1-x}\text{Cu}_x\text{O}_3$ thin films ($x = 0.0, 0.2, 0.3$ and 0.5).

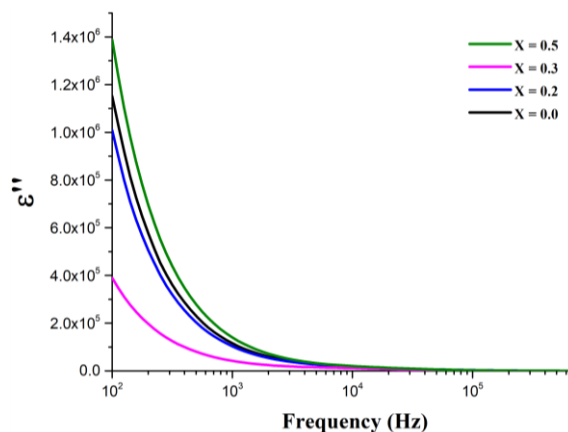


Figure 7. Frequency dependence of imaginary dielectric permittivity (ϵ'') of $\text{BiFe}_{1-x}\text{Cu}_x\text{O}_3$ thin films ($x = 0.0, 0.2, 0.3$ and 0.5).

3.2. Electrical properties

The dielectric permittivity constant (ϵ^*) and loss tangent ($\tan\delta$) were used to evaluate the electrical properties of the Cu-doped BiFeO_3 ($x = 0.0, 0.2, 0.3$ and 0.5) thin films. The ϵ^* and $\tan\delta$ are shown in figures 6 and 7. Figure 6 shows an increase in the real dielectric permittivity constant of $\text{BiFe}_{1-x}\text{Cu}_x\text{O}_3$ thin films with an increase of Cu content over the measured frequency range, except when $x = 0.3$ to $x = 0.5$ suddenly decreased. Conversely, the imaginary dielectric permittivity constant decreases with an

increase in Cu content and it suddenly increases at $x = 0.5$ as shown in figure 7. Moreover, the dielectric permittivity constant increases as the crystallite size decreases (from 2.92 nm to 2.57 nm) for the $x = 0.0$ to $x = 0.3$ samples, respectively. Generally, the decreases in the dielectric constant in the ferrite-based nanoparticles such as BiFeO_3 or Fe_3O_4 are due to material preparation by doping which produces an aggregation of small crystallite sizes [4-5]. Similarly, the dielectric constant of the Cu-doped BiFeO_3 thin films in this work decreases which can be attributed to the decreases in crystallite size that cause large insulating barriers to charge carrier mobility [4-5].

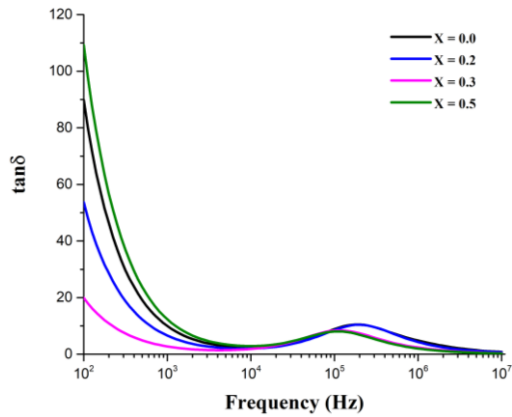


Figure 8. Frequency dependence of $\tan\delta$ of $\text{BiFe}_{1-x}\text{Cu}_x\text{O}_3$ thin films ($x = 0.0, 0.2, 0.3$ and 0.5).

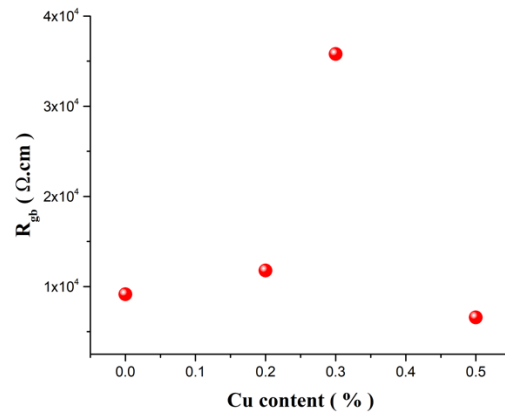


Figure 9. Grain boundary resistance (R_{gb}) versus Cu content of $\text{BiFe}_{1-x}\text{Cu}_x\text{O}_3$ thin films ($x = 0.0, 0.2, 0.3$ and 0.5).

Figure 8 shows the $\tan\delta$ values depend on Cu content, which can be attributed to the great electric conductivity of copper. The grain boundary resistance (R_{gb}) of the thin films as shown in figure 9 were calculated by using the dielectric permittivity constant and loss tangent values [9-10, 12, 17-18]. The R_{gb} of the thin films are 9.1, 11.7, 35.7 and 6.5 $\text{k}\Omega\cdot\text{cm}$ for $x = 0.0, 0.2, 0.3$ and 0.5 , respectively, which increase with increases in Cu content. The grain boundary resistance of the $x = 0.3$ sample reaches the maximum value. Clearly, this increase in R_{gb} may be due to the effect of decreases in crystallite size. Moreover, the grain boundary conductivity (σ_{gb}) was calculated by $\sigma_{gb} = \frac{1}{R_{gb}}$ [2, 11-12, 17]. The calculated grain boundary conductivity values of the thin films are 1.1×10^{-4} , 0.8×10^{-4} , 0.2×10^{-4} and 1.5×10^{-4} S/cm for $x = 0.0, 0.2, 0.3$ and 0.5 samples, respectively. Clearly, the decreases in the crystallite size with higher Cu content for $x = 0$ to $x = 0.3$ causes decreases in the σ_{gb} values. Moreover, Cu-doping at $x = 0.5$ which was the largest crystallite size (3.44 nm) exhibits the highest values of the grain boundary conductivity.

4. Conclusions

The $\text{BiFe}_{1-x}\text{Cu}_x\text{O}_3$ thin films (where $x = 0.0, 0.2, 0.3$ and 0.5) were successfully fabricated by a spin coating technique. The phase structure and morphology of the thin films were characterized by the XRD and SEM methods. The oxidation state of Fe and Cu ions was confirmed by the XAS method. The electrical properties of the dielectric permittivity constant and the loss tangent were studied. The results show that Cu-doping of BiFeO_3 thin films can cause increases in the grain boundary resistance and dielectric permittivity constant, which are related to decreases in the loss tangent or decreases in the electrical properties. Clearly, Cu-doping can affect crystallite size which can influence the electrical properties of the Cu-doped BiFeO_3 thin films.

Acknowledgments

The author would like to thank all the contributors, including Suranaree University of Technology, Synchrotron Light Research Institute (BL 5.2), Nakhon Ratchasima, Thailand for the XAS facility, the

Department of Physics, Faculty of Science, Khon Kaen University, Khon Kaen, Thailand, for measurement of electrical properties, and the Development and Promotion of Science and Technology Talents Project for the support of this M.Sc. study. This research is financially supported by the SUT CoE on Advanced Functional Materials (SUT-AFM), Suranaree University of Technology.

References

- [1] Qi X, Roberts P S, Mathur N D, Lee J S, Foltyn S, Jia Q X and MacManus-Driscoll J L 2006 *Advanced Dielectric, Piezoelectric and Ferroelectric Materials* ed. Tuttle B A, Chen C, Jia Q and Ramesh R (Indianapolis: Indiana) pp. 69–73
- [2] Liu G Z, Wang C, Wang C C, Qian J, He M, Xing J, Jin K J, Lu H B and Yang G Z 2008 *Appl. Phys. Lett.* **92** 122903
- [3] Wang X, Yan B, Dai Z, Liu M and Liu H 2010 *Ferroelectrics* **410** 96–101
- [4] Lopez Maldonad K L, De La Presa P, De La Rubia M A, Crespo P, De Frutos J, Hernando A, Matutes Aquino J A and Elizalde Galindo J T 2014 *J. Nanopart. Res.* **16** 2482
- [5] Dhir G, Uniyal P and Verma N K 2017 *Phys. Status Solidi C* **14** 1600253
- [6] Dong G, Tan G, Luo Y, Liu W, Xia A and Ren H 2014 *Appl. Surf. Sci.* **305** 55–61
- [7] Zhai X Z, Deng H M, Zhou W L, Yang P X, Chu J H and Zheng Z 2015 *RSC Adv.* **5** 82351–56
- [8] Khajonrit J, Phumying S and Maensiri S 2016 *Jpn. J. Appl. Phys.* **55** 06GJ14
- [9] Qian G, Zhu C, Wang L, Tian Z, Yin C, Li C and Yuan S 2017 *J. Electron. Mater.* **46** 6717–26
- [10] Wu X, Tian M, Guo Y, Zheng Q, Luo L and Lin D 2015 *J. Mater. Sci. Mater. Electron.* **26** 978–84
- [11] Zhou J P, Yan P L, Xiao R J, Chen X M and Deng C Y 2012 *Mater. Res. Bull.* **47** 3630–36
- [12] Rivera R., Hejazi M and Safari A 2012 *Proc. ISAF-ECAPD-PFM* 12981022
- [13] Khajonrit J, Prasoesopha N, Sinprachim T, Kidkhunthod P, Pinitsoontorn S and Maensiri S 2017 *Adv. Nat. Sci. Nanosci. Nanotechnol.* **8** 015010
- [14] Khajonrit J, Wongpratrat U, Kidkhunthod P, Pinitsoontorn S and Maensiri S 2018 *J. Magn. Magn. Mater.* **449** 423–34
- [15] Xue J M, Sim M H, Ezhilvalavan S, Zhou Z H, Wang J, Zhu H and Miao J M 2004 *Thin Solid Films* **460** 1–6
- [16] Ravel B and Newville M 2005 *J. Synchrotron Radiat.* **12** 537
- [17] Boonlakhom J, Thongbai P, Putasaeng B, Yamwong T and Maensiri S 2014 *J. Alloy. Compd.* **612** 103–9
- [18] Riaz S, Shah S M H, Akbar A, Atiq S and Naseem S 2015 *J. Sol-Gel Sci. Techn.* **74** 329–39